APS physics

CHORUS

This is the accepted manuscript made available via CHORUS. The article has been published as:

Edge currents and nanopore arrays in zigzag and chiral graphene nanoribbons as a route toward high-ZT thermoelectrics

Po-Hao Chang and Branislav K. Nikolić

Phys. Rev. B **86**, 041406 — Published 16 July 2012

DOI: 10.1103/PhysRevB.86.041406

Edge currents and nanopore arrays in zigzag or chiral graphene nanoribbons as a route toward high-ZT thermoelectrics

Po-Hao Chang and Branislav K. Nikolić*
Department of Physics and Astronomy, University of Delaware, Newark, DE 19716-2570, USA

We analyze electronic and phononic quantum transport in zigzag or chiral graphene nanoribbons (GNRs) perforated with an array of nanopores. Since local charge current profiles in these GNRs are peaked around their edges, drilling nanopores in their interior does not affect edge charge currents while drastically reducing phonon heat current in sufficiently long wires. The combination of these two effects can yield highly efficient thermoelectric devices with maximum $ZT \simeq 5$, at both liquid nitrogen and room temperature achieved, in ~ 1 μm long zigzag GNRs with nanopores of variable diameter and spacing between them. Our analysis is based on the nonequilibrium Green function formalism combined with the π-orbital tight-binding Hamiltonian with up to third nearest-neighbor hopping for electronic subsystem, or with empirical fifth-nearest-neighbor force-constant (5NNNFC) model for phononic subsystem. Additionally, we demonstrate that different empirical FC models typically overestimate the phonon conductance when compared to first-principles results.

PACS numbers: 85.80.Fi, 72.80.Vp, 73.63.-b, 81.07.Gf

The recent explosion of research on graphene—one-atom-thick allotrope of carbon—has been largely focused on its unique electronic structure and transport properties governed by the two-dimensional honeycomb lattice of carbon atoms.[1] Very recently, the exploration of its thermal and thermoelectric properties has been initiated by measuring the thermopower[2] S and phonon thermal conductivity[3] $\mathcal{K}_{\rm ph}$ of large-area graphene. The measured values[2] of $S \simeq 100$ μV/K near the Dirac point (DP), as well as the room-temperature $\mathcal{K}_{\rm ph} \simeq 4000$ W/mK (averaged over values obtained using different samples and experimental techniques[3]) which outperforms virtually all other known materials, point out that large-area graphene is *not suitable* for thermoelectric applications.

Thermoelectrics transform temperature gradients into electric voltage and vice versa. Although a plethora of thermoelectric energy harvesting and cooling applications has been envisioned, their usage is presently limited by their small efficiency.[4] Thus, careful tradeoffs are required to optimize the dimensionless figure of merit $ZT = S^2GT/(\kappa_{\rm el} + \kappa_{\rm ph})$ which quantifies the maximum efficiency of a thermoelectric cycle conversion in the linear-response regime where a small voltage $V = -S\Delta T$ exactly cancels the current induced by the small thermal bias ΔT. This is due to the fact that ZT contains unfavorable combination of S, average temperature T, electronic conductance G and thermal conductance $\kappa_{\rm el}+\kappa_{\rm ph}$. The total thermal conductance has contributions from both electrons $\kappa_{\rm el}$ and phonons $\kappa_{\rm ph}$. The devices with $ZT > 1$ are regarded as good thermoelectrics, but values of $ZT > 3$ are required for thermoelectric devices to compete in efficiency with conventional power generators and refrigerators.[4]

Thus, a number of proposals have been put forth to evade the problem of high lattice thermal conductivity of large-area graphene that could open a pathway for its thermoelectric applications. For example, large-area graphene could reach $ZT \approx 0.3$ if perforated by the so-called antidot lattice tailored to impede phonon propagation.[5] Switching to quasi-one-dimensional graphene nanoribbons (GNRs) makes possible further enhancement of ZT where it has been predicted that long (~ 1 μm) GNRs with zigzag edges and *disorder* introduced around edges by removing carbon atoms could reach $ZT \simeq 4$ at room temperature.[6] Another route is to engineer structural defects in GNRs that can block phonons while retaining quasiballistic electronic transport.[7]

However, it is more advantageous to search for high-ZT devices among nanowires[8] with well-defined edges since edge or surface disorder can affect electronic conductance significantly. For example, the experiments on etched GNRs with rough edges find Coulomb blockade effects (not taken into account in Ref. 6) and transport gap much larger than the band gap.[9]

In this Rapid Communication, we exploit the peculiar electronic transport properties of GNRs with zigzag (ZGNR) or chiral (CGNR) edges, illustrated in Fig. 1, where the local charge current density carried by quasiparticles sufficiently close to the DP is peaked around nanoribbons edges as demonstrated in Fig. 2(b) and (c). Thus, drilling nanopores[10] in the ZGNR or CGNR interior will not substantially modify such "edge currents." This is confirmed in Fig. 2 using spatial profiles of bond currents, as well as by the transmission function in Figs. 3(a) and 3(c) which is reduced from $\mathcal{T}_{\rm el}(E) = 3$ in infinite homogeneous GNRs to $\mathcal{T}_{\rm el}(E) \simeq 2$ around the DP for both ZGNR and CGNR with an array of nanopores. Furthermore, $\mathcal{T}_{\rm el}(E)$ around the DP does not change as one increases the length of GNRs because "edge currents" propagate quasiballistically.

The nanopore arrays have been explored before[11] in bulk thermoelectric materials. Furthermore, their fabrication in graphene has been pursued recently by a variety of experimental techniques.[10] Since they break homogeneity of the nanowire, they can substantially impede the propagation of phonons in sufficiently long GNRs. This is corroborated by our results for the phonon transmission function in Figs. 4(a) and 4(b) and the

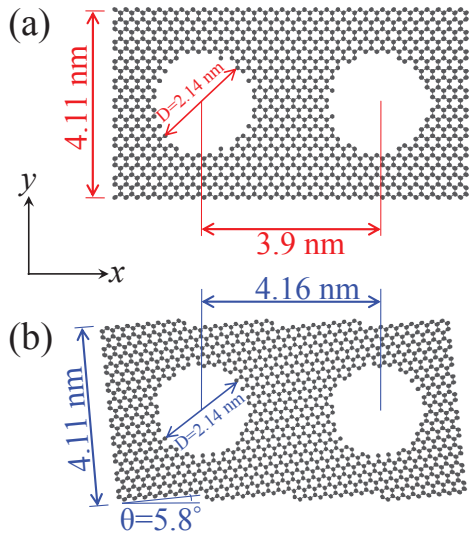

FIG. 1: (Color online) Schematic view of: (a) 20-ZGNR (composed of 20 zigzag chains); and (b) (8,1)-CGNR with chiral angle $\theta = 5.8^\circ$. The size of the nanopores, assumed to be drilled in the GNR interior away from its zigzag or chiral edges, and the distance between them is illustrated by plotting two repeated supercells of each GNR. The length of these GNRs in the actual calculations is set to $L \simeq 1.2$ μm which supports 300 nanopores.

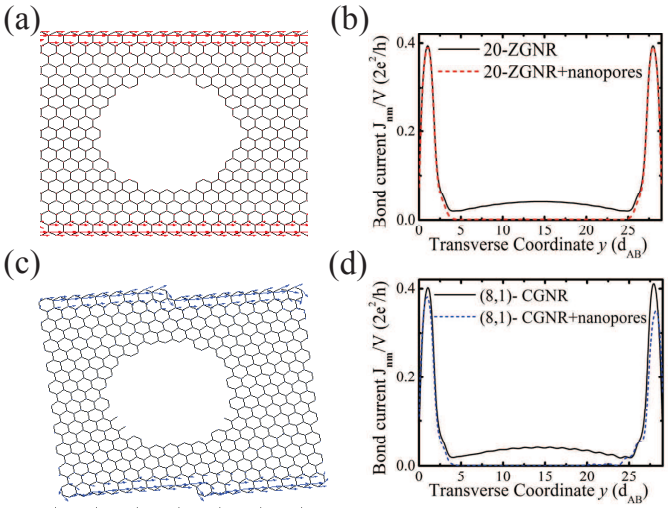

FIG. 2: (Color online) Spatial profiles of local charge currents in (a) 20-ZGNR and (c) (8,1)-CGNR with nanopores for electronic transport close ($E_F = -0.43$ eV) to the DP. The corresponding current profiles over the transverse cross section of nanoribbons are shown in panels (b) and (d) for both infinite homogeneous GNRs and GNRs with nanopores. Note that the sum of bond currents[15] $J_{\mathbf{nm}}/V$, which describe charge flow from site $\mathbf{n}$ to site $\mathbf{m}$ of the honeycomb lattice if hopping $t_{\mathbf{n}}^{\mathbf{m}} \neq 0$ is non-zero between the two sites, gives the conductance $G = I/V$ (I is the total current in the leads and $V \to 0$ is small bias voltage driving the linear-response transport).

corresponding lattice thermal conductance in Figs. 4(c) and 4(d). The ZGNR and CGNR length is chosen as $L \simeq 1.2$ μm, which is close to the limit beyond which further increase of L does not reduce $\kappa_{\rm ph}$ significantly. The number of nanopores hosted by GNRs of these length is 300.

Combining these two effects, we obtain maximum $ZT \simeq 4$ at $T = 77$ K and $ZT \simeq 2$ at $T = 300$ K in Fig. 5(a) for the case of 20-ZGNR whose identical nanopores are arranged in a periodic array. The values of ZT for (8,1)-CGNR with periodic array of nanopores are lower, as shown in Fig. 5(c). In realistic GNR-based devices, it may be challenging[10] to control the pore arrangement to a high precision assumed in Fig. 1. Therefore, in Figs. 5(b) and 5(d) we assume that the pore diameter D is a uniform random variable, such as $D \in [4.5\,d_{AB}, 7.5\,d_{AB}]$ for pores in 20-ZGNR or $D \in [1.5\,d_{AB}, 3.5\,d_{AB}]$ for pores in (8,1)-CGNR, as well as that position of nanopores is shifted randomly by $\Delta x \in [-2\,d_{AB}, 2\,d_{AB}]$ in 20-ZGNR or $\Delta x \in [-0.5\,d_{AB}, 0.5\,d_{AB}]$ in (8,1)-CGNR where $d_{AB} \approx 0.142$ nm is the C-C bond length. This yields maximum value of $ZT \simeq 5$ in our study, at both $T = 77$ K and $T = 300$ K, as shown in Fig. 5(b).

In the rest of the paper we explain details of our models for electronic and phononic subsystems, which are coupled to nonequilibrium Green function formalism (NEGF) to treat their elastic quantum transport.[12] The early theoretical studies of ZGNR-based devices have utilized[13] a simplistic tight-binding model (TBM) with single π-orbital per site and the nearest-neighbor hopping only, or its long-wavelength (continuum) approximation—the Dirac-Weyl Hamiltonian[14]—valid close to the DP. However, both of these models predict[13,15] that the transmission function of an infinite homogeneous ZGNR is $\mathcal{T}_{\rm el} = 1$ around the DP and that current density profile is peaked[15] in the middle of ZGNR (even though local density of states reaches maximum around the edges[15]). This contradicts first-principles calculations,[16] or TBM with up to third nearest-neighbor[17] hopping parameters fitted to such first-principles calculations, which predict $\mathcal{T}_{\rm el} = 3$ around the DP, as well as that the local current density is mostly confined to flow around the zigzag edges.[18] It is worth mentioning that the majority of recent studies focused on the thermoelectric properties of ZGNRs with edge disorder[6] or finite length graphene antidot lattice[5] have utilized the TBM with nearest-neighbor hopping, so that a possibility to exploit "edge currents" around zigzag or chiral edges for thermoelectric device applications has been *overlooked*.

Most importantly, the recent experiments have confirmed the existence of "edge currents" in metallic ZGNRs by actually utilizing them to increase the heat dissipation around edge defects and, thereby, rearrange atomic structure locally until sharply defined zigzag edge is achieved.[19] Also, the very recent chemical synthesis[20] of (8,1)-CGNRs via carbon nanotube unzipping method have exhibited properties in sub-nanometer-

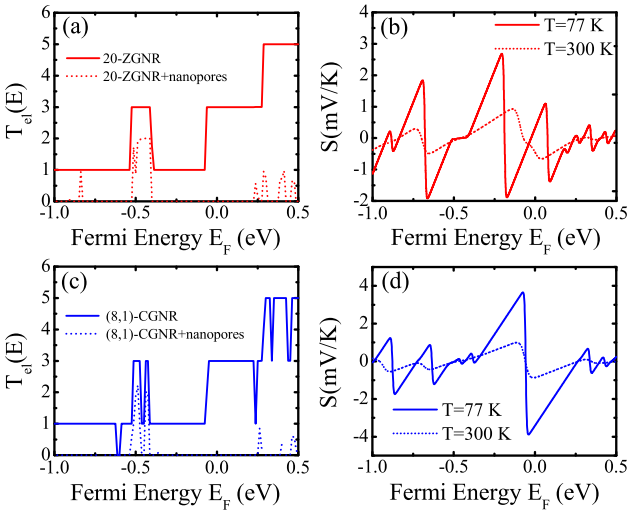

FIG. 3: (Color online) The zero-bias electronic transmission $\mathcal{T}_{\rm el}(E)$ for: (a) infinite homogeneous 20-ZGNR or finite length 20-ZGNR with periodic array of identical nanopores shown in Fig. 1(a); and (c) infinite homogeneous (8,1)-CGNR or finite length (8,1)-CGNR with periodic array of identical nanopores shown in Fig. 1(b). Panels (b) and (d) show the the thermopower at two different temperatures corresponding to finite length 20-ZGNR with nanopores in panel (a) or finite length (8,1)-CGNR with nanopores in panel (c), respectively.

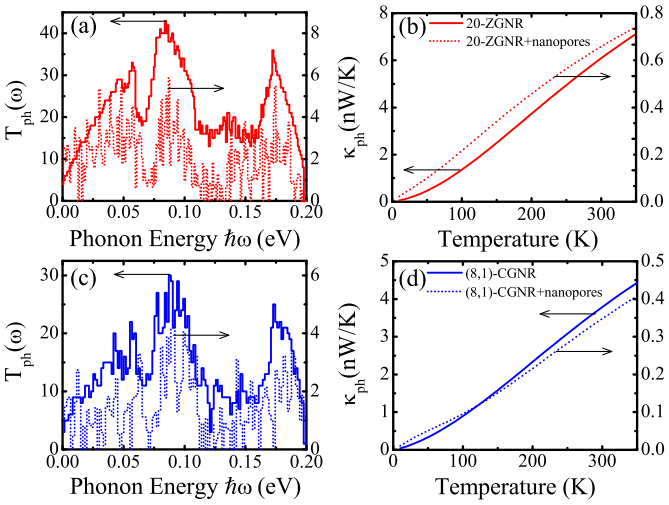

FIG. 4: (Color online) (a) The phonon transmission function $\mathcal{T}_{\rm ph}(\omega)$ and (b) the corresponding phonon thermal conductance $\kappa_{\rm ph}$ for an infinite homogeneous 20-ZGNR or 20-ZGNR with periodic array of identical nanopores shown in Fig. 1(a). (c) The phonon transmission function and (d) the corresponding phonon thermal conductance $\kappa_{\rm ph}$ for an infinite homogeneous (8,1)-CGNR or (8,1)-ZGNR with a periodic array of identical nanopores shown in Fig. 1(b).

resolved scanning tunneling microscopy and spectroscopy that can only be explained by the existence of smooth edges supporting edge quantum states (i.e., wavefunctions whose probability density is large around the edges). Although ZGNRs[21] or CGNRs[20] are insulating at very low temperatures due to one-dimensional spin-polarized edge states coupled across the width of the nanoribbon, such unusual magnetic ordering and the corresponding band gap is easily destroyed[21] above $T \gtrsim 10$ K.

We adopt the TBM with single π-orbital per site:

$$\hat{H} = \sum_{\mathbf{n}} \varepsilon_{\mathbf{n}} \hat{c}^{\dagger}_{\mathbf{n}} \hat{c}_{\mathbf{n}} - \sum_{\mathbf{n},\mathbf{m}} t^{\mathbf{m}}_{\mathbf{n}} \hat{c}^{\dagger}_{\mathbf{n}} \hat{c}_{\mathbf{m}}, \qquad (1)$$

to describe the electronic subsystem of 20-ZGNR and (8,1)-CGNR in Fig. 1. The operators $\hat{c}^{\dagger}_{\mathbf{n}}$ ($\hat{c}_{\mathbf{n}}$) create (annihilate) electron in the π-orbital located on site $\mathbf{n}$ of the honeycomb lattice whose lattice constant is $a \approx 0.246$ nm. For impurity-free GNRs assumed here, the on-site potential is set to zero $\varepsilon_{\mathbf{n}} = 0$. We consider up to third nearest-neighbor[17] hopping parameters—$t^{\mathbf{n}+\mathbf{d}_{AB}}_{\mathbf{n}} = 2.7$ eV, $t^{\mathbf{n}+\mathbf{d}_{AA}}_{\mathbf{n}} = t^{\mathbf{n}+\mathbf{d}_{BB}}_{\mathbf{n}} = 0.2$ eV, and $t^{\mathbf{n}+\mathbf{d}_{AB'}}_{\mathbf{n}} = 0.18$ eV—which describe the nearest-, next-nearest- and next-next-nearest neighbor hopping, respectively. Since the honeycomb lattice of graphene is composed of two triangular sublattices A and B, the parameters $t^{\mathbf{n}+\mathbf{d}_{AB}}_{\mathbf{n}}$ and $t^{\mathbf{n}+\mathbf{d}_{AB'}}_{\mathbf{n}}$ describe intersublattice hopping, while $t^{\mathbf{n}+\mathbf{d}_{AA}}_{\mathbf{n}} = t^{\mathbf{n}+\mathbf{d}_{BB}}_{\mathbf{n}}$ describes the intrasublattice hopping.

In realistic devices, active region consisting of ZGNR or CGNR of finite length with nanopores will eventually need to be connected to metallic electrodes. However, since GNR+nanopores devices we analyze are rather long ~ 1 μm, and screening takes place over a distance much shorter than the active region, it is justified to use semi-infinite homogeneous ZGNRs or CGNRs as leads for simplicity.

In the elastic transport regime, where electron-phonon and phonon-phonon scattering can be neglected, independent electron and phonon transport quantities can be obtained from NEGF-based formulas whose technical details can be found in Ref. 12. This methodology does not take into account the resistive umklapp phonon-phonon scattering which plays an important role in interpretation of experiments on room-temperature lattice thermal conductivity of large-area graphene.[3] However, this effect, which is easy to describe using the Boltzmann equation but is very expensive computationally within the NEGF formalism,[22] does not play an important role in GNRs depicted in Fig. 1 because their width is much smaller than the mean-free path $\ell \simeq 677$ nm due to phonon-phonon scattering in large-area graphene at room temperature.[23]

The widely used methodology to compute $\kappa_{\rm ph}$ of GNRs couples[6,24] NEGF to empirical fourth-nearest-neighbor force-constant[25] (4NNFC) or 5NNNFC[26] models. The parameters of 4NNNFC and 5NNNFC models have been refined over the years to reproduce the newly acquired experimental data on the phonon dispersion of graphite,[26] fit DFT calculations[25] for infinite graphene sheets, and

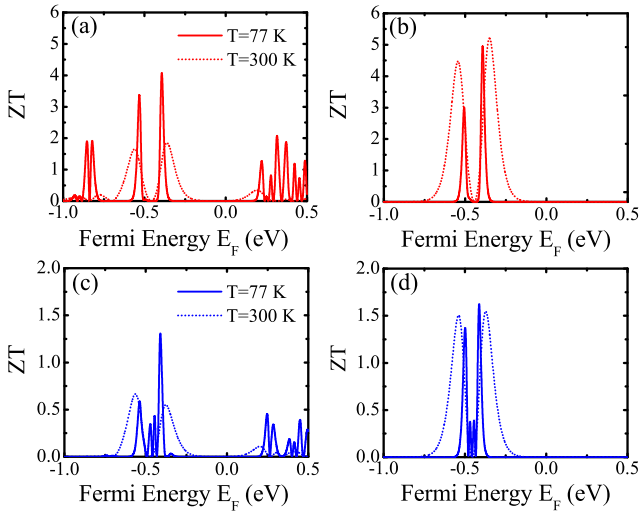

FIG. 5: (Color online) The thermoelectric figure of merit ZT vs. energy at two different temperatures for (a),(b) ZGNR+nanopores and (c),(d) CGNR+nanopores. In panels (a) and (c) we assume a periodic array of identical nanopores, as illustrated in Fig. 1, while in panels (b) and (d) the nanopore diameter and the distance between neighboring pores is a uniform random variable. The curves plotted in panels (b) and (d) are computed for a single sample.

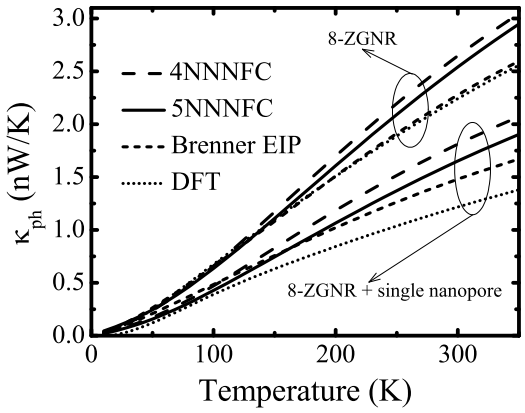

FIG. 6: The phonon thermal conductance as a function of temperature for 8-ZGNR with and without a single nanopore (of diameter $D = 0.59$ nm) computed by coupling NEGF formalism to empirical 4NNNFC,[25] empirical 5NNNFC,[26] Brenner EIP,[29] and DFT (using the basis of local DZP orbitals and PBE exchange-correlation functional). The FC matrix in the case of Brenner EIP and DFT methodology was computed using the GPAW package.[27]

satisfy the symmetry imposed conditions (such as rotational invariance[25]). However, direct application of these models to GNRs is not warranted since force constants on the edge carbon atoms will be modified when compared to those in their interior. While the resulting shift in the phonon density of states and the corresponding reduction of $\kappa_{\rm ph}$ are typically assumed to lead only to a minor improvement,[6] here we explicitly compare $\kappa_{\rm ph}$ obtained from these models to first-principles calculations. We also include the Brenner empirical interatomic potential[29] (EIP) which offers much faster numerics than full DFT methodology while being able to match the DFT results for some device geometries.[5,12]

The first-principles extraction of the FC matrix $\mathbf{K}$ is performed via the GPAW package,[27] which is a real space electronic structure code based on the projector augmented wave method.[28] The electronic wavefunctions are expanded in atomic orbitals with a double-zeta polarized (DZP) basis set, and Perdew-Burke-Ernzerhof (PBE) parametrization of the generalized gradient approximation for the exchange-correlation functional is used. The whole active region, composed of a segment of 8-ZGNR with or without a nanopore and few layers of the semi-infinite 8-ZGNR leads, is first relaxed to a maximum force of 0.01 eV/Å per atom. Subsequently, we displace each atom I by $Q_{I\alpha}$ in the direction $\alpha = \{x, y, z\}$ to get the forces $F_{J\beta}(Q_{I\alpha})$ on atom $J \neq I$ in direction β. The elements of $\mathbf{K}$-matrix are then computed from finite differences $K_{I\alpha,J\beta} = [F_{J\beta}(Q_{I\alpha}) - F_{J\beta}(-Q_{I\alpha})]/2Q_{I\alpha}$. The intra-atomic elements are calculated by imposing momentum conservation, such that $K_{I\alpha,I\beta} = -\Sigma_{J\neq I} K_{I\alpha,J\beta}$. In the case of Brenner EIP-based calculation, we initially relax the active region and then compute the force constant between atom I in direction and atom J in direction β using analytical derivatives, $K_{I\alpha,J\beta} = \partial U/(\partial R_{I\alpha}\partial R_{J\beta})$, where U is the total energy. These calculations are also performed using the GPAW package.[27]

Since calculations based on 4NNNFC and 5NNNFC models do not include passivation of edge carbon atoms with (usually assumed) hydrogen, we do not include hydrogen atoms in DFT- or Brenner EIP-based analysis. This approximation is further justified by the first-principles results of Ref. 30 where ZGNRs with and without hydrogen-passivation exhibit virtually the same $\kappa_{\rm ph}$ due to the fact that edge C-C bonds are only slightly perturbed in the presence of hydrogen.

The comparison of different $\kappa_{\rm ph}$ values, computed by coupling NEGF to four different FC matrices in Fig. 6, shows that *all three empirical models* overestimate the phonon thermal conductance of ZGNR+nanopore when compared to first-principles result. In the case of an infinite homogeneous ZGNR, Brenner EIP and DFT calculations yield virtually the same $\kappa_{\rm ph}$ in Fig. 6, while 4NNNFC and 5NNNFC models lead to an overestimate of this quantity. While the first-principles calculations of $\kappa_{\rm ph}$ are too expensive to be applied to our $L \simeq 1.2$ μm GNRs (that are also wider than the 8-ZGNR example used in Fig. 6), the comparison of different methods applied to a testbed in Fig. 6 demonstrates that actual ZT or the proposed ZGNR and CGNR devices will be even higher than the one computed in Fig. 5 using 5NNNFC model.

In conclusion, we predicted that ZGNRs and CGNRs perforated by an array of nanopores in their interior could serve as the building blocks of highly efficient thermoelectric devices. This is due to the fact that local charge current density is peaked around their edges, as demonstrated explicitly by Fig. 2 and confirmed experimentally,[19] so that nanopores do not impede such "edge currents" while drastically reducing phonon conduction in sufficiently long ZGNRs or CGNRs. In the case of periodic array of identical nanopores, we find that largest $ZT \simeq 4$ at $T = 77$ K and $ZT \simeq 2$ at $T = 300$ K can be reached using ZGNR-based devices. On the other hand, if the pore diameter takes a random value within some interval and the distance between the pores is varied, then we find a possibility of even higher figure of merit which can reach $ZT \simeq 5$ at both $T = 77$ K and $T = 300$ K in the case of ZGNR+nanopores devices.

Acknowledgments

We thank T. Markussen and V. Meunier for illuminating discussions. Financial support from NSF under Grant No. ECCS 1202069 is gratefully acknowledged.

* Electronic address: bnikolic@udel.edu

[1] A. K. Geim, Science **324**, 1530 (2009).
[2] Y. M. Zuev, W. Chang, and P. Kim, Phys. Rev. Lett. **102**, 096807 (2009).
[3] A. A. Balandin, Nature Mater. **10**, 569 (2011).
[4] C. B. Vining, Nature Mater. **8**, 83 (2009).
[5] T. Gunst, T. Markussen, A.-P. Jauho, and M. Brandbyge, Phys. Rev. B **84**, 155449 (2011).
[6] H. Sevinçli and G. Cuniberti, Phys. Rev. B **81**, 113401 (2010).
[7] J. B. Haskins *et al.*, ACS Nano **5**, 3779 (2011).
[8] T. Markussen, A.-P. Jauho, and M. Brandbyge, Phys. Rev. Lett. **103**, 055502 (2009).
[9] F. Molitor *et al.*, Semicond. Sci. Technol. **25**, 034002 (2010).
[10] J. W. Bai *et al.*, Nature Nanotech. **5**, 190 (2010); K. Tada *et al.*, Phys. Rev. Lett. **107**, 217203 (2011).
[11] J-H. Lee, G. Galli, and J. Grossman, Nano Lett **8**, 3750 (2008); Y. He, D. Donadio and G. Galli, Nano Lett. **11**, 3608 (2011); O. A. Tretiakov, Ar. Abanov, and J. Sinova, Appl. Phys. Lett. **99**, 113110 (2011).
[12] B. K. Nikolić, K. K. Saha, T. Markussen, and K. S. Thygesen, J. Comp. Electronics **11**, 78 (2012).
[13] A. Rycerz, J. Tworzydło, and C. W. J. Beenakker, Nature Phys. **3**, 172 (2007).
[14] L. Brey and H. A. Fertig, Phys. Rev. B **73**, 235411 (2006).
[15] L. P. Zârbo and B. K. Nikolić, Europhys. Lett. **80**, 47001 (2007).
[16] K. K. Saha, M. Drndić, and B. K. Nikolić, Nano Lett. **12**, 50 (2012).
[17] A. Cresti *et al.*, Nano Research **1**, 361 (2008); Y. Hancock *et al.*, Phys. Rev. B **81**, 245402 (2010);
[18] D. Areshkin and C. White, Nano Lett. **7**, 3253 (2007).
[19] X. Jia *et al.*, Science **323**, 1701 (2009).
[20] C. Tao *et al.*, Nature Phys. **7**, 616 (2011).
[21] O. V. Yazyev and M. I. Katsnelson, Phys. Rev. Lett. **100**, 047209 (2008); J. Kunstmann, C. Özdoğan, A. Quandt, and H. Fehske, Phys. Rev. B **83**, 045414 (2011).
[22] N. Mingo, Phys. Rev. B **74**, 125402 (2006).
[23] Z. Aksamija and I. Knezevic, Appl. Phys. Lett. **98**, 141919 (2011).
[24] F. Mazzamuto *et al.*, J. Appl. Phys. **109**, 064516 (2011).
[25] J. Zimmermann, P. Pavone, and G. Cuniberti, Phys. Rev. B **78**, 045410 (2008).
[26] M. Mohr *et al.*, Phys. Rev. B **76**, 035439 (2007).
[27] https://wiki.fysik.dtu.dk/gpaw/.
[28] J. Enkovaara *et al.*, J. Phys.: Condens. Matter **22**, 253202 (2010).
[29] D. W. Brenner, Phys. Rev. B **42**, 9458 (1990).
[30] Z. W. Tan, J.-S. Wang, and C. K. Gan, Nano Lett. **11**, 214 (2010).